Fermi National Accelerator Laboratory

FERMILAB-Conf-89/264-E
[E-741/CDF]

Small Angle Physics at CDF: A Progress Report *

The CDF Collaboration

presented by

Riccardo Paoletti
Instituto Nazionale di Fisica Nucleare - Sezione di Pisa
56010 S. Piero a Grado, Pisa, Italy

December 16, 1989

* Talk presented at the 8th Topical Workshop on $p\bar{p}$ Collider Physics, Castiglione della Pescaia, Italy, September 1-5, 1989.

Operated by Universities Research Association Inc. under contract with the United States Department of Energy

CDF/MIN_BIAS/PUB/CDFR/1075
December 16, 1989

Small Angle Physics at CDF: A Progress Report

The CDF Collaboration[1]

Presented by *Riccardo PAOLETTI*
Istituto Nazionale di Fisica Nucleare – Sezione di Pisa
56010 S. Piero a Grado, Italy
at the 8^{th} Workshop on Proton-Antiproton Collider Physics
Castiglione della Pescaia (GR), Italy, 1-5 September 1989

Abstract

In 1989 CDF collected data in special high beta runs with a trigger selecting elastic and inelastic events in order to measure the total cross section (σ_{tot}) and the differential elastic cross section ($d\sigma_{el}/dt$). Data were taken at cms energies of 300, 540, 1000 and 1800 GeV. A double arm magnetic spectrometer located along the beam pipe tags the particles scattered at very small angles and tracking detectors surrounding the interaction point reveal particles produced at larger angles. We discuss the status of the analysis of elastic and inelastic events with emphasis on the event selection and the background subtraction.

1 The Physics Program

The main goal of the experiment is to measure the total cross section. By using the optical theorem, the total cross section is given by

$$(1+\rho^2)\sigma_{tot} = 16\pi(\hbar c)^2 \frac{(dR_{el}/dt)_{t=0}}{R_{el}+R_{inel}}$$

where ρ is the ratio of the real to the imaginary part of the forward scattering amplitude and R_{el} and R_{inel} are the elastic and inelastic (including both diffractive and non diffractive processes) rates. Elastic and inelastic events are produced in different angular regions that are covered with two experimental setups, respectively called the elastic and the inelastic detectors.

[1]ANL-Brandeis-University of Chicago-Fermilab-INFN,Frascati-Harvard-University of Illinois-KEK-LBL- University of Pennsylvania-INFN,University and Scuola Normale Superiore of Pisa-Purdue-Rockefeller-Rutgers-Texas A&M-Tsukuba-University of Wisconsin

2 The Measurement of Elastic Events

Most of elastically scattered particles are produced at angles smaller than 1 mrad. Detectors must be close to the beam. A particle produced with a 300 μrad angle is detected after 30 m at about 1.0 cm from the beam center.

We have installed the detectors, called "stations", in five Tevatron warm sections. They are located left and right of the interaction region between collider magnets as shown in fig.1. In every station two "Roman pots" can be moved toward the beam in the horizontal plane. The motion is remotely controlled with a position reproducibility of the order of 10 μm. The detectors are kept outside the beam pipe during injection and acceleration. Once beams have been conveniently scraped, pots are moved in. Pot positions must be determined every time because the beam orbit can change from store to store.

Every pot (fig.2) is equipped with two trigger scintillators, a four-cell drift chamber and a silicon crystal. Every drift cell has a vertical sense wire. The chamber is operated with an Ar-Ethane mixture (50:50) and a drift field of 1.1 kV/cm. The drift time measures the horizontal position with respect to the beam. The vertical position is measured by inducing a delay line parallel to the sense wires. The performance of these chambers has been studied by using a sample of elastic tracks. A resolution of 120 μm in the horizontal position and 800 μm in the vertical position is achieved [1].

The silicon crystal anode is segmented in vertical strips 50 μm wide with a 500 μm pitch. The horizontal position is measured by using the charge division method. The silicon cathode is divided in horizontal strips, 1 mm wide, to measure the vertical position. The performance of these crystals was studied in a Fermilab test beam [2]. We measured a 60 μm resolution for the horizontal coordinate and a 300 μm resolution for the vertical one. In the experiment, however, the horizontal resolution was measured to be 150 μm. The silicon was in particular useful to determine the two unknown constants that relate the absolute horizontal position to the chamber drift time, *i.e.* the drift velocity and the t_0. The data taking periods were distant in time and the chamber operating conditions varied accordingly. A measurement of the drift velocity for every run allows us to reduce the systematic error in the position measurement (a 200 μm error in the reconstructed coordinate would correspond to a 1% change in drift velocity). In addition the use of two independent detectors to measure the position of the same particle results in a very high reconstruction efficiency (>99%, discussed below).

2.1 Selection of Elastic Events

In fig.3 we see what an elastic event looks like in our apparatus. The two scattered particles travel in opposite directions and hit the pots on opposite sides. The trigger requires the coincidence of the scintillator signals in all the pots on opposite sides

with respect to the interaction point. With the notation indicated in the figure the two elastic triggers are:

(	S1_out	*	S2_out	*	S3_out	*	S6_in	*	S7_in	)	"arm 0"
(	S1_in	*	S2_in	*	S3_in	*	S6_out	*	S7_out	)	"arm 1"

In some runs we required the coincidence of S3 only with S6*S7 to extend the spectrometer acceptance that it is limited by the beam pipe between S3 and S2.

The elastic trigger accepts not only good events but also random coincidences of beam halo particles travelling parallel to the beam axis (fig.4), one going in the direction of S1, S2 and S3 while the other hits stations S6 and S7. The characteristics of these halo events are different from the elastic (fig.3). When projected in the horizontal plane back to the interaction region, elastic particles are at small distance x_o from the beam line (the beam spot is $\simeq$ 500μm). If we plot the production angle θ_o versus the impact parameter x_o, we expect elastic events to be clustered in a vertical band corresponding to small impact parameters (rectangles in fig.5). On the contrary the beam halo particles will be spread all along x_o and almost parallel to the beam ($\theta_o \simeq 0$). The data indeed show this expected behaviour (fig.5). The diagonal cut visible in this figure is caused by the geometrical acceptance.

To determine the scattering angle we need to know the position of the pots relative to the beam axis. The pots positions can be extracted from our data using both elastic and beam halo events. In fact, elastic events allow us to align the chambers on opposite arms and beam halo events to align the chambers on the same side of the ring. On the other hand, we also surveyed the position of our detectors and, in particular, we measured the distance between two detectors in the same station with an accuracy of 100 μm.

It turns out that, in order to align the spectrometers with elastic and halo particles, the distance between detectors in stations S6 and S7 has to be about 500 μm smaller than what actually measured by survey. This disagreement, probably due to the use of not accurate enough transport matrices describing the Tevatron lattice, reduces our confidence in the angular measurement. It is however worth noting that it is only the redundancy built into the experiment that allows us to measure this discrepancy. At the moment, we are working on this problem and we do not present a measurement of the elastic differential cross section.

With the pot positions, as found from the data, we analyzed a data sample consisting of ~17000 elastic triggers, which corresponds to about 15% of the data collected at $\sqrt{s}$ =1.8 TeV. The following cuts were applied to clean the data sample (table 1):

1) Beam halo removal: events in which a track in pots 1,2,3 matches a track in pots 6,7 on the same side are removed because they are attributed to a halo particle traveling parallel to the beam.

2) Multiplicity cut: 3311 events have such a high particle multiplicity in either S1 and S2, or S6 and S7 that chambers in those pots are completely unusable. This makes it impossible to apply the cuts described below and all these events have been rejected. Indeed, none of these events is a good elastic as it is shown in the detailed analysis of appendix A.

3) Minimal elastic requirement: we ask for at least one track, on both sides, compatible with coming from the interaction vertex.[2]

4) Vertex cut: in order to remove the halo particles faking the elastic signal from the sample, we make a cut on the production angle and impact parameter of tracks on the S1,S2 and S3 side (solid lines in fig.5). The collinearity distribution for events rejected by this cut is shown in fig.6.

5) Finally, a cut at $\pm$ 3σ is applied to the collinearity distribution (fig.7). From the tails of the same distribution we estimate the background under the peak to be less than 5%.

The result is summarized in table 1.

Table 1: Elastic events selection

	# events passing the cut	# elastic events lost by the cut
All elastic triggers	16993	
Remove clear halo	12671	≤ 2
Cut on high multiplicity	9360	$\simeq 0$
Minimal elastic requirement	6546	≤ 10 in the West arm (all in S3) ≤ 17 in the East arm
Vertex requirement x_o vs θ_o	5253	≤ 2
3σ collinearity cut in $\Delta\theta_x$	4961	≤ 3
		Total event loss ≤ 34 ($\leq 1\%$)

All the above cuts reduce the initial data sample by a factor 3, while losing less than <1% of the good events. We determined the number of lost elastic events by looking at the collinearity distribution of the discarded events and estimating the excess of events around $\Delta\theta_x$=0.

[2] In some cases we were left with more than one track passing this selection. In this case we chose the East/West pair with the best collinearity. We checked that these pairs were indeed elastic candidates by proving that their collinearity distribution is narrower than the one obtained by making the same choice East/West tracks from different events.

We define a fiducial region (table 2) in which both the chamber and the trigger are 100% efficient. The measured angular distribution in this region has been corrected for the geometrical acceptance. It is shown in fig.8. The solid line is an exponential fit performed in the range $0.05<|t|<0.20$.

Table 2: Fiducial region for acceptance correction

Vertical coordinate $\|Y\| \leq 1$ cm Horizontal coordinate $\|X\| \geq \|X\|_{cathode} + 500\mu m$	chamber and trigger full efficiency cuts
Production angle $\theta_o \leq 500\mu$rad ($\|t\| \leq 0.202$ (GeV/c)^2)	Beam pipe acceptance cut

3 The Measurement of the Inelastic Rate

The measurement of the total cross section requires extrapolation to full solid angle of the inelastic rate. The events that are most likely to be lost are those where all particles are confined to small angles. Therefore we measure tracks down to 2 mrad.

The inelastic detector (fig.9) consists of chambers and scintillators. On both sides of the interaction region, angles from 90° down to 2 mrad are covered by using:

1) the Vertex Time Projection Chamber (VTPC) [3] (from 90° down to ~60 mrad)

2) Two telescopes, consisting of 16 planar drift chambers, inherited from the UA4 experiment [4] (from ~60 to ~8 mrad)

3) Stations S4 and S5. Each station consists of two sets of movable pots, one below and one above the beam line, which can be pushed vertically toward the beam by a pneumatic drive. Each set contains a telescope of two drift chambers, 90 cm apart, similar to those used in the elastic spectrometer. A scintillation counter, set behind every chamber, is used for triggering. These detectors, once in position, cover from ~8 to ~2 mrad.

As a trigger we used two sets of scintillation counters:

1) the Beam Beam Counters (BBC) [5] covering from ~78 mrad down to ~5 mrad.

2) The previously described scintillators in stations S4 and S5 covering from ~8 to ~2 mrad.

We 'OR'ed the BBC and pot scintillation counters on each side thus defining a 'single arm' trigger. The trigger used for inelastic events was the EAST*WEST coincidence of the two single arms, while to explore the diffractive events we made a coincidence of each single arm trigger with a small angle spectrometer trigger. More precisely the diffractive triggers were:

Single_Arm_East AND ((S1_out AND S2_out) OR (S1_in AND S2_in))

Single_Arm_West AND ((S6_out AND S7_out) OR (S6_in AND S7_in))

Different prescaling factors have been applied to the various triggers in order to get comparable statistics. Typical values were 16 for the inelastic trigger, 8 & 2 for the WEST and EAST diffractive triggers, respectively.

Fig.10a shows an inelastic candidate event as seen by the VTPC. Fig.10b shows the same event as seen by the UA4 chambers.

To check the performance of the UA4 chambers we selected a sample of events with a good vertex in the VTPC and reconstructed the vertex position along the beam with the UA4 chambers only. Fig.11 shows the correlation between the vertices found by the VTPC and by the UA4 chambers. The difference has a width of 13 cm, while the interaction region is about 1m long (fig.12). We expect the UA4 chambers to have the same performance in single diffractive events or in events where the VTPC information is not available because all the tracks were below its angular coverage.

3.1 Selection of Inelastic Events

A large fraction of the inelastic data sample is background caused by beam gas or beam pipe interactions. We have two ways of removing it:

1) A Time Of Flight (TOF) cut. We reject events in which one of the small angle scintillator (in S4 or in S5) was hit by particles in time with the incoming beam. Fig.13 shows the time spectrum of one of these counters. We can easily distinguish the peak due to particles coming from the interaction vertex and the peak due to particles early in time.

2) A VTPC reconstruction quality cut. Background events are characterized by lots of hits in the VTPC not associated with any reconstructed track. These hits are caused by streams of particles crossing the VTPC (fig.14). A simple cut on the number of reconstructed tracks versus the number of hits in the chamber removes a large fraction of this background.

Table 3 shows the selection flow. Two points are worth notice:

1) in 25% of the cases we need the information of the UA4 chambers because the VTPC alone was not able to find a good vertex.

2) The last cut in table 3 rejects 19 events. 9 are clearly background, 10 have no information from either VTPC or the UA4 chambers. To understand these events we must add the information from the S4 and S5 chambers that we have just begun to study.

Table 3: Inelastic events selection (on one tape)

	# events	# lost events (from VTPC vertex distribution and visual scan)
All double arm triggers	2262	
Time Of Flight filter	612	≤ 3
VTPC hit/track ratio	558	≤ 2
Vertex reconstruction (UA4 + VTPC)	539	≤ 5
		Total event loss ≤ 10 ($\leq 2\%$)

The rejection power of these cuts is evident from figs. 15b-15c. They show the VTPC vertex distribution for events passing the TOF and the VTPC quality cuts. Figs. 15d-15e show the same distributions for rejected events. Work is in progress to determine more accurately the efficiency of this selection.

4 Conclusions

The analysis of small angle data collected by the CDF collaboration is in progress. We are making use of the redundancy and precision of the magnetic spectrometer in order to reduce the systematic uncertainties of the elastic scattering measurement. We are not quoting any result at this time due to the still incomplete understanding of the magnetic spectromter alignment and to the fact that the analysis of the inelastic events is still in an early stage.

References

[1] S. Bertolucci *et al.*, *The small angle spectrometer of CDF*, presented by G. Chiarelli at the 3rd Pisa Meeting on Advanced Detectors for Advanced Physics, La Biodola, Elba (Italy) May 1989

[2] G. Apollinari *et al*, IEEE Transactions on Nucl. Sci. **36** (1989) 46.

[3] F. Snider *et al*, Nucl. Instr. Meth. **A268** (1988) 75-91.

[4] A. Bechini *et al*, Nucl. Instr. Meth. **156** (1978) 181.

[5] F. Abe *et al*, Nucl. Instr. Meth. **A271** (1988) 387-403.

Appendix A

We explain why there are no elastic events among those 3311 rejected by the multiplicity cut (table 1).

In 293 events, S1 and S2 have too many hits to be useful. We can still use S3, S6 and S7 to check the collinearity of the two sides (the track production angles are calculated in this case by imposing the vertex constraint x_o=0). An excess of 40 events was found in the region $\mid \Delta\theta_x \mid < 60\mu$rad. These events all have production angle $\theta_o > 500\mu$rad, *i.e.* beyond the acceptance limit defined by the beam pipe diameter. The high hit multiplicity in S1 and S2 is easily explainable as nuclear interactions in the beam pipe.

In the other 3018 events, where S6 and S7 have too many hits and are therefore unusable, the collinearity check is not possible. There we use the power of the S1, S2 and S3 spectrometer only. In 1284 events the track in the West side does not pass the vertex cut. 837 events are classified as inelastic by inspection of the inelastic detector trigger counters (see par. 3.1). Since S1, S2 and S3 cover angles smaller than S6 and S7, we expect most of the remaining events to be due to interactions of elastic particles with the thick pot bottom of S6 or S7. By using the information of S1, S2 and S3 we extrapolated the impact point of the particle to S6. In 769 events this point falls on the pot bottom region (this number of events is consistent with the extrapolation of the final elastic angular distribution in this region). The remaining 128 events have a flat x_o distribution and they are compatible with random coincidences between beam halo in the West side and beam gas in the East side.

293	high multiplicity in S1,S2 (West side)
1284	West track not passing vertex cut
837	trigger counters pattern consistent with inelastic trigger
769	interaction of particles with the pot bottom
128	beam halo in S1, S2 and S3
3018	high multiplicity in S6,S7 (East side)
3311	total number of events rejected by the multiplicity cut

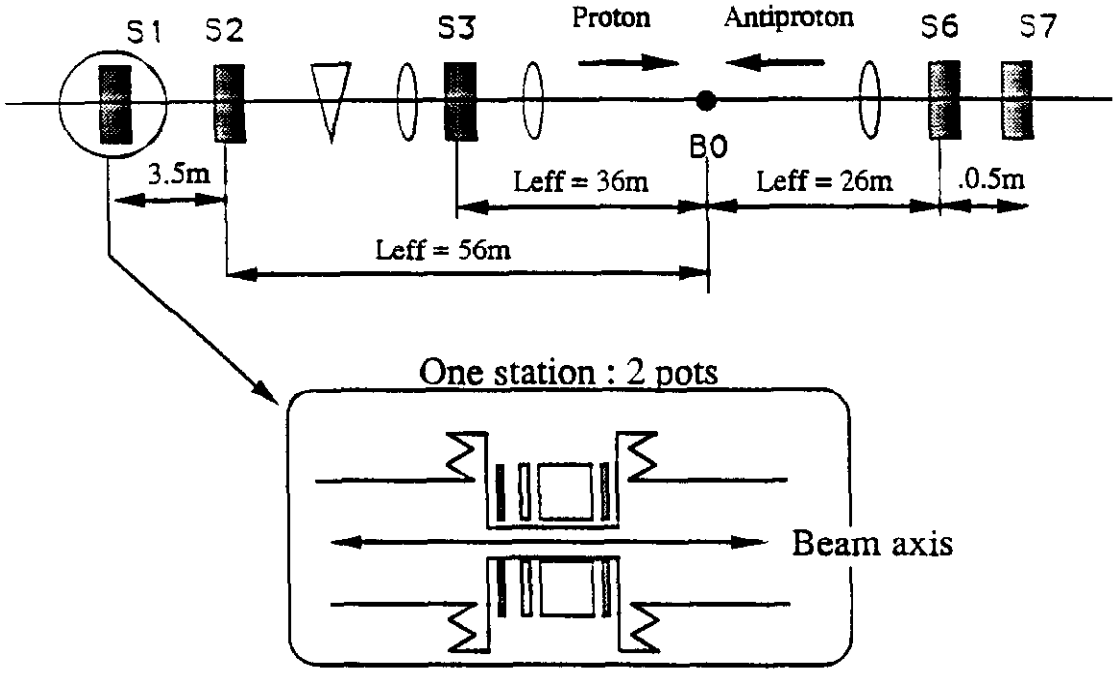

Fig.1 Top views of the elastic detector showing the location of the stations in the Tevatron tunnel (a) and the pots inside one station (b).

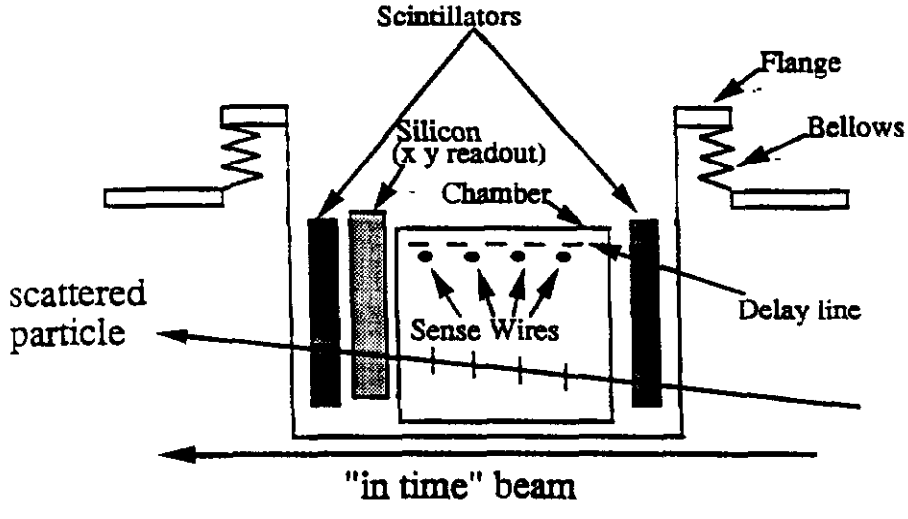

Fig.2 Schematic view of the pot assembly.

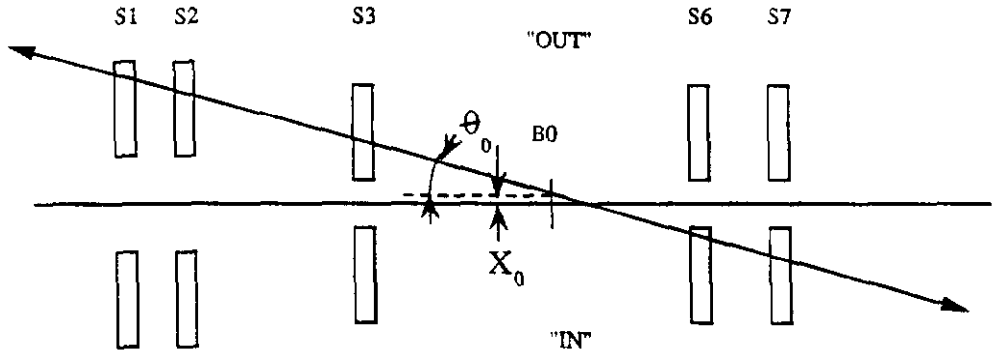

Fig.3 Characteristic track production angle and impact parameter for elastic tracks.

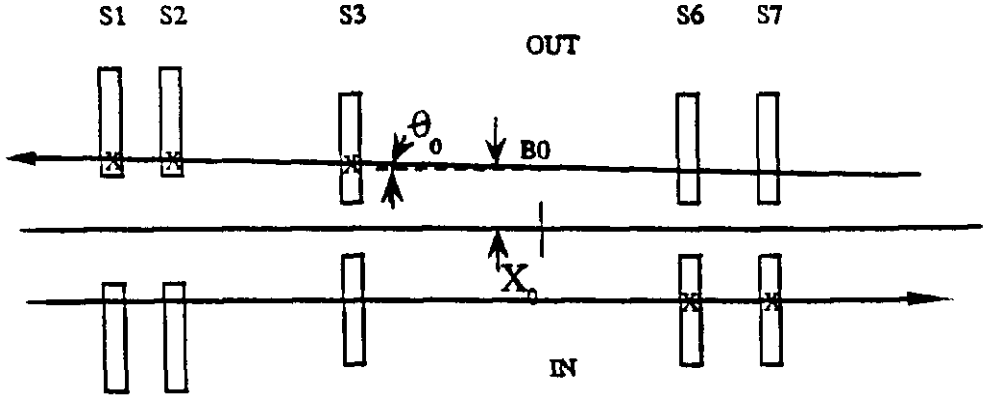

Fig.4 Same as Fig.3 for beam halo tracks.

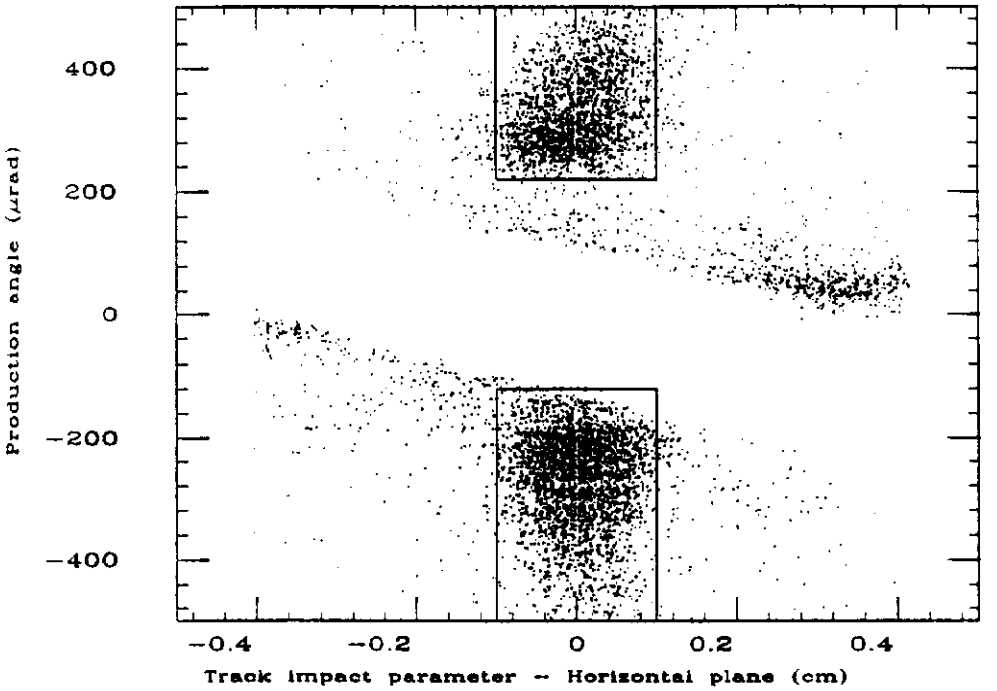

Fig.5 Scatter plot of the track production angle vs the track impact parameter. The rectangles represent the vertex cut used in the elastic data sample selection (see table 1). Elastic data are expected to lie inside those regions.

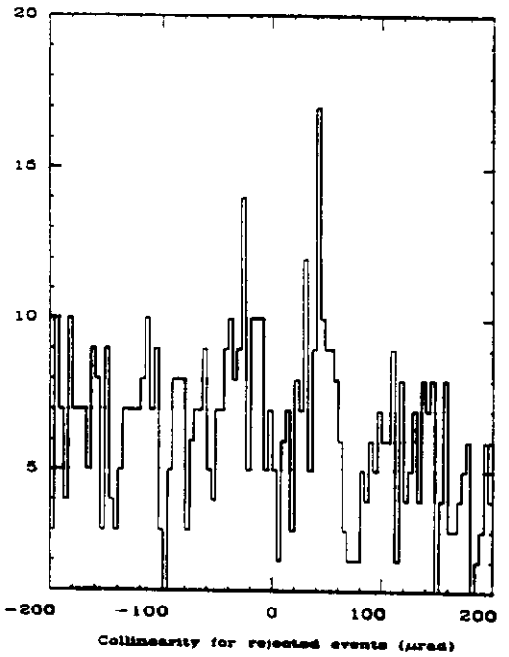

Fig.6 Collinearity distribution for events rejected by the vertex cut.

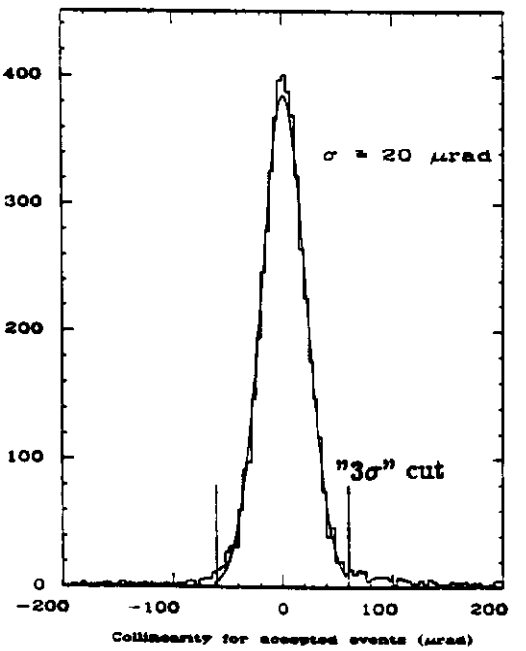

Fig.7 Collinearity distribution for events passing the vertex cut.

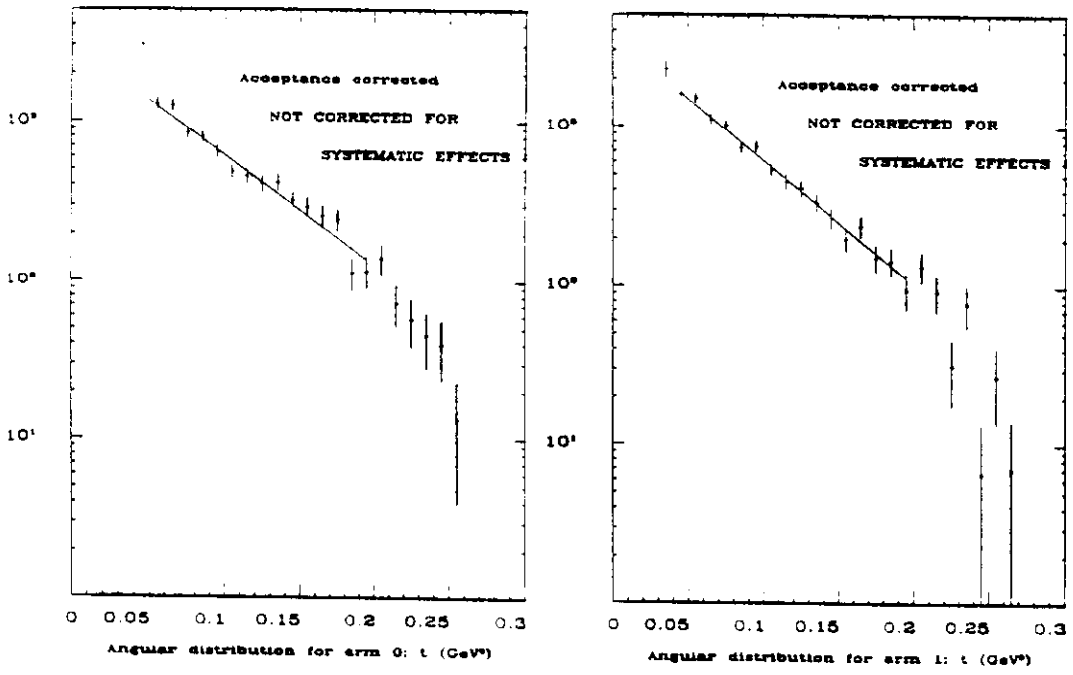

Fig.8 Final angular distributions of elastic events for arm 0 (a) and arm 1 (b).

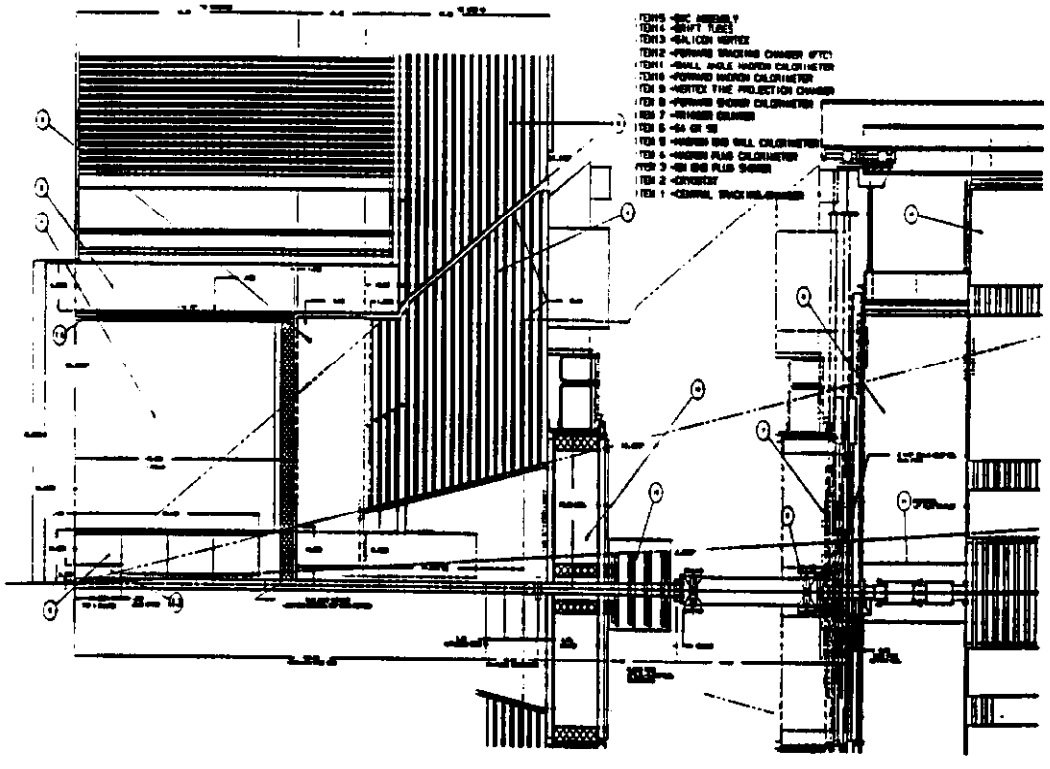

Fig.9 Side view of the inelastic detector.

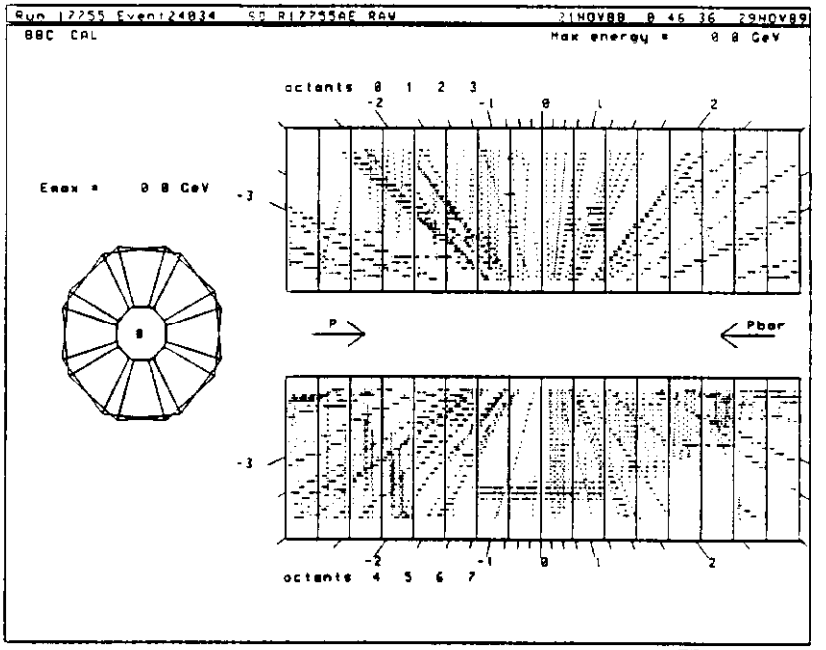

Fig.10 Side view of an inelastic event in the VTPC (a)

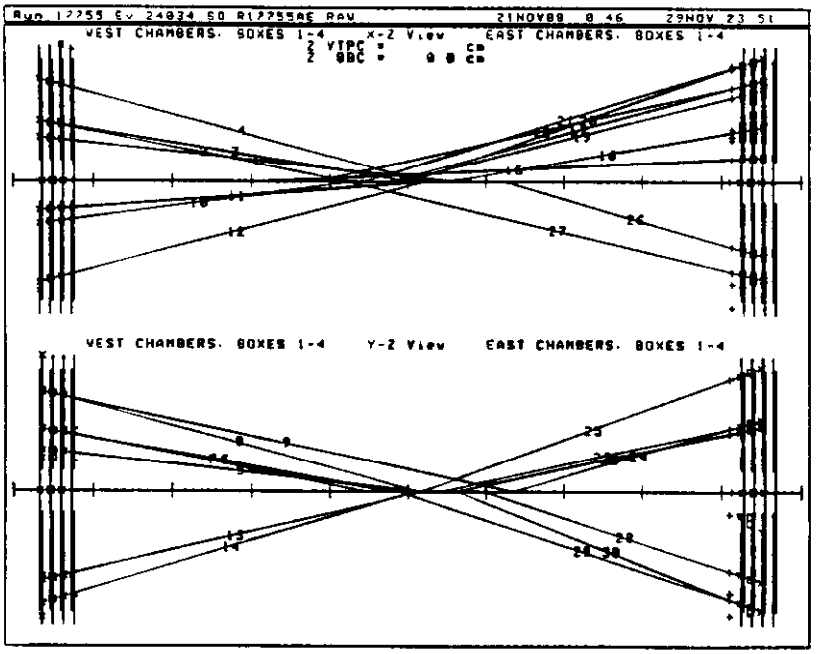

and in the UA4 chambers (b).

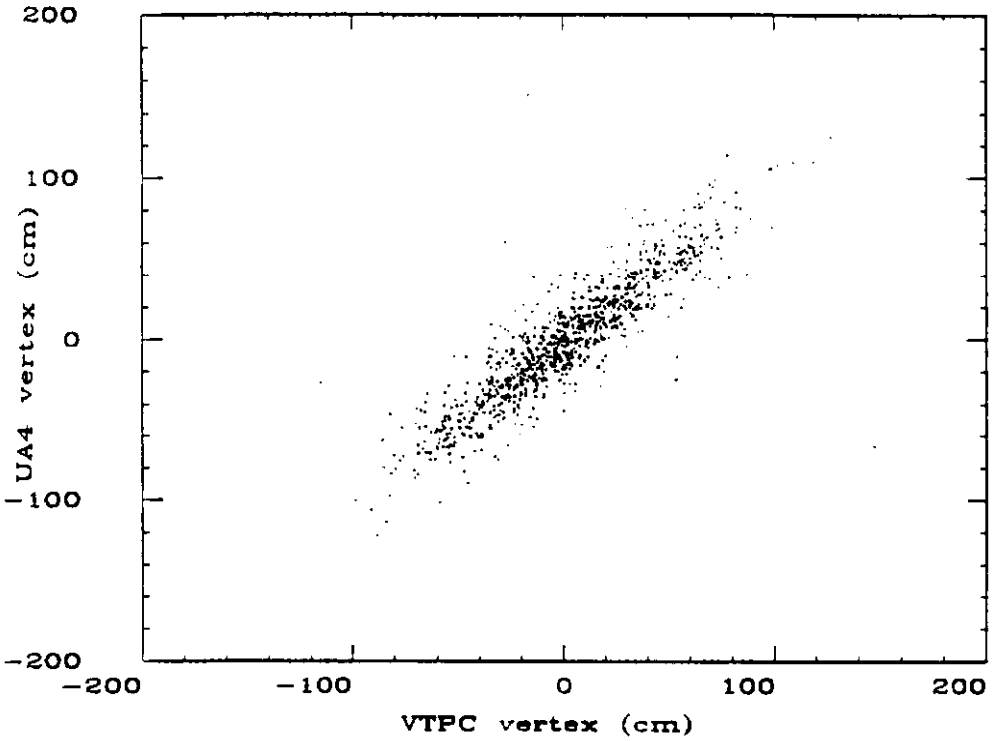

Fig.11 Correlation between the vertices found with the VTPC and the UA4 chambers.

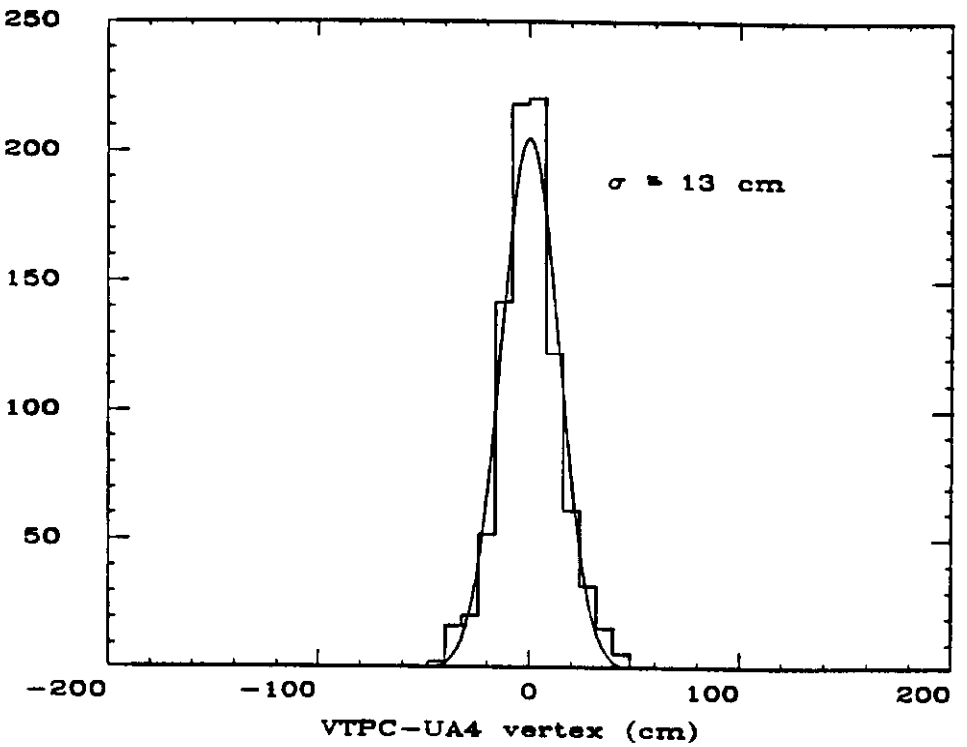

Fig.12 Difference of the vertex coordinate found with the VTPC and the UA4 chambers.

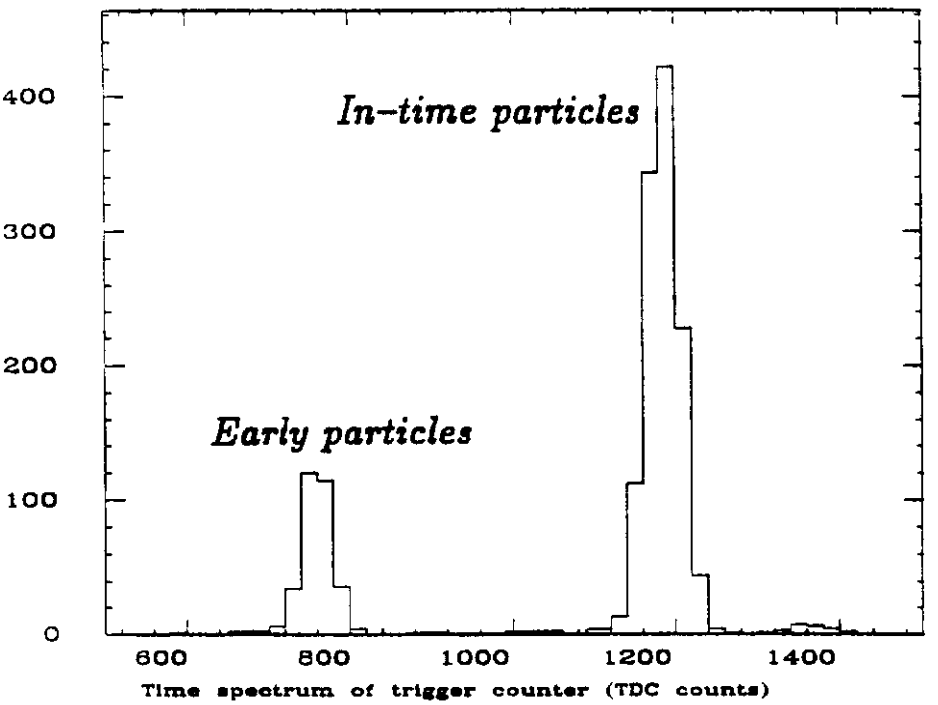

Fig.13 Time spectrum of one of the counters installed in stations S4 and S5. Clearly visible are the peak of in-time particles and of early particles. Also visible is the signal of satellite bunches. The horizontal scale is arbitrary.

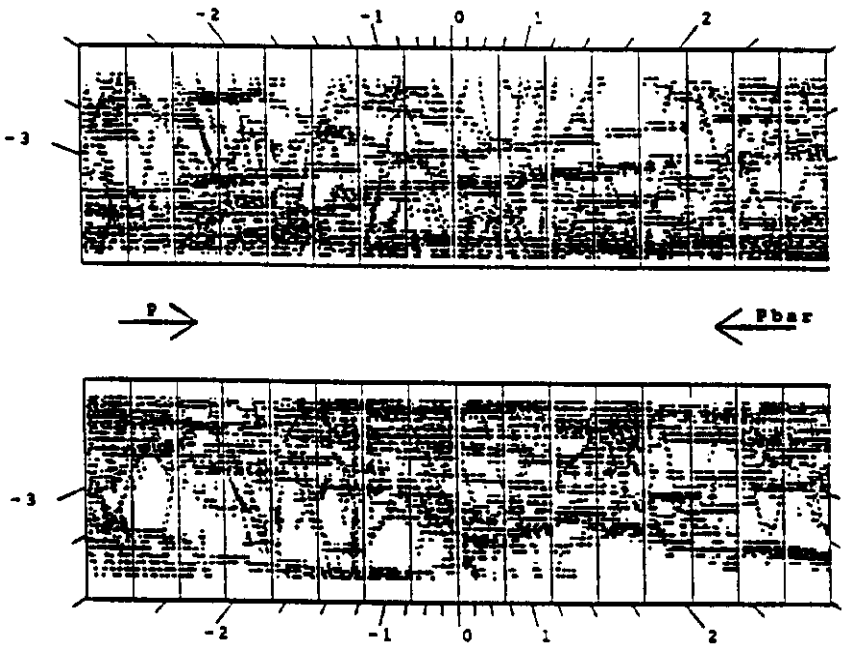

Fig.14 A beam-gas event as seen by the VTPC. Note the stream of particles traversing the entire volume of the chamber.

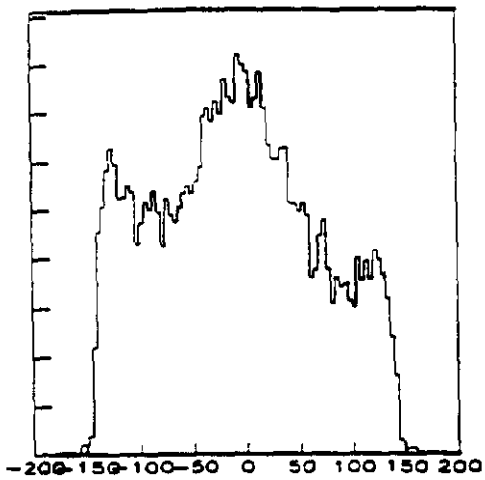

Raw VTPC vertex distribution (a)

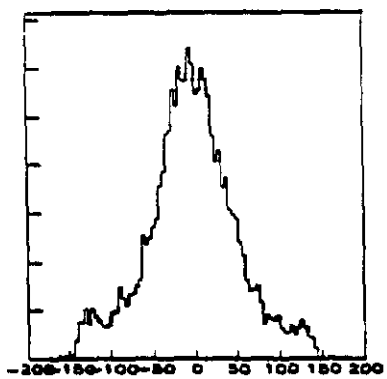

events passing TOF cut (b)

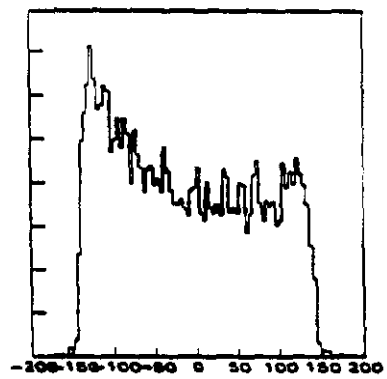

rejected by TOF cut (d)

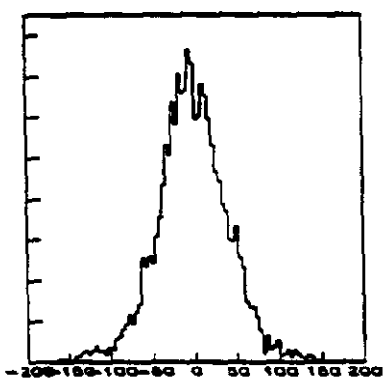

passing TOF + VTPC cut (c)

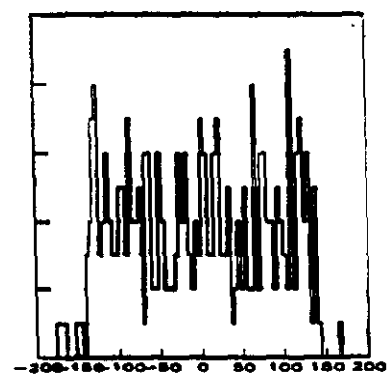

passing TOF cut but rejected by VTPC cut (e)

Fig.15 Sequence of VTPC vertex distributions after the cuts used in the clean-up of inelastic triggers.